Materials Chemistry and Physics 160 (2015) 111–118

Contents lists available at ScienceDirect

Materials Chemistry and Physics

journal homepage: www.elsevier.com/locate/matchemphys

Development of titania nanotube arrays: The roles of water content and annealing atmosphere

Ratnawati [a, c], Jarnuzi Gunlazuardi [b], Slamet [a, *]

[a] Chemical Engineering Department, Faculty of Engineering, Universitas Indonesia, Depok 16424, Indonesia
[b] Chemistry Department, Faculty of Mathematics and Science, Universitas Indonesia, Depok 16424, Indonesia
[c] Chemical Engineering Department, Institut Teknologi Indonesia, Tangerang Selatan 15320, Indonesia

HIGHLIGHTS

- Water content of 25 v%, annealing with 20% H_2 produced highest photocurrent of TNTAs.
- Vertically oriented, long with optimal wall thickness of TNTAs increase photocurrent.
- Annealing with H_2/Ar plays an effective role in reducing the band gap.

ARTICLE INFO

Article history:
Received 4 March 2014
Received in revised form
3 April 2015
Accepted 6 April 2015
Available online 15 April 2015

Keywords:
Annealing
SEM
EDS
FTIR

ABSTRACT

The effect of water content in the electrolyte solution during annealing process in the synthesis and modification of titania nanotube arrays (TNTAs) by anodic oxidation process has been investigated. Variations in annealing technique that leading to some specific properties of the TNTAs produced have been examined. Doped-TNTAs were obtained by the in-situ anodic oxidation method in glycerol containing fluoride solution followed by annealing to induce crystallization. FESEM and SEM results indicated that TNTAs with inner diameters of 49–80 nm, wall thicknesses from 28 to 42 nm and lengths from 1407 to 1570 nm were synthesized. At water content of 25 v% in the electrolyte solution, self-organized with vertical, ordered of TNTAs with relatively uniform diameter was observed. Suitable morphology of TNTAs such as well developed tubes, vertically oriented, highly ordered, long with optimal diameter and wall thickness of TNTAs could suppress recombination of electrons–holes and, therefore, increase photoelectrochemical properties. Annealing with H_2/Ar is found to be efficient for introducing dopant C and N into the lattice of TNTAs to form Ti–O–C and N–Ti–O (FTIR analysis). Therefore, the reducing band gap can be obtained (UV–Vis DRS analysis). Annealing under H_2/Ar of as-synt TNTAs with water content of 25 v% in the electrolyte solution produced anatase phase (XRD analysis) and showed optimal condition in producing the highest photocurrent density.

1. Introduction

TiO_2 is one of the most promising photocatalysts and has attracted much attention due to its advantages such as non-toxicity, stability, environmental harmlessness and low cost [1–6]. Activation of this photocatalyst needs photon energy, which can be provided by solar light at ambient condition instead of thermal energy. This photocatalyst has many applications such as being a photocatalyst in H_2 production [1,3], pollutant degradation [3–8], dye-sensitized solar cells (DSSC) [3,9] and even in sanitation and cancer therapy [10]. However, TiO_2 has several drawbacks such as photoinduced electron–hole recombination [1,2], visible light inactivity (band gap of TiO_2: 3.2 eV for anatase, 3.0 eV for rutile) [1–9] and limited surface area [1,11,12]. Consequently, its utilization efficiency especially in solar light is still poor as the UV portion accounts for only about 5% while visible light accounts for about 45% in solar spectra [2,4,5,8,13]. Hence, some modification strategies need to be examined to reduce those drawbacks of TiO_2 such as morphology modifications (to increase the surface area), addition of non-metal doping (to extend the photo-responsiveness to the visible light) or metal doping (to minimize recombination of

* Corresponding author.
E-mail addresses: rnwt63@yahoo.co.id (Ratnawati), jarnuzi@ui.ac.id (J. Gunlazuardi), slamet@che.ui.ac.id (Slamet).

http://dx.doi.org/10.1016/j.matchemphys.2015.04.013
0254-0584/

electron–hole) and coupling with other semiconductors such as CdS [11].

Many attempts to alleviate those drawbacks have been studied, and one of them is synthesizing TiO_2 by anodic oxidation of titanium metal in order to get morphology of TiO_2 nanotube arrays that have larger surface area compared to the randomly distributes and shape nanoparticles [3,11,12]. TiO_2 synthesized by the anodic oxidation process (TNTAs) exhibit better properties than TiO_2 in a randomly distributes and shape nanoparticles system as morphology of TNTAs enhances photon absorption, effectively increases the surface area and provides excellent electron–hole separation properties [11,12]. Accordingly, the morphology of the TNTAs can improve performance in its photoactivity. Formation of TNTAs in organic electrolyte such as glycerol with high viscosity result in a low growth rate of nanotube since the tube growth rate is a diffusion-controlled process [11,14]. However, extending anodization time resulted in the increasing the tube length. Magnetically stirring during the anodization process can be used to enhance the mass transfer of the ions inside the solution and therefore increase the growth rate. The smooth wall that improves properties of TNTAs is another interesting result of anodization in glycerol electrolyte solution [11]. Furthermore, decreasing the viscosity by adding the various water content into glycerol electrolyte solution plays an important role in determining the optimum growth rate, dimension and the morphology of TNTAs. As a result, the specific properties that improve the characteristics of TNTAs caused by variation in water content during anodization can be obtained.

Doping TiO_2 with non-metal such as C [4,6,8], N [1,3–6,13], B [2,8], I [5] and co-doping with N+S [3], C+N [4,6], C+B [8] and N+I [5] has been demonstrated to reduce the band gap, thus improving its photocatalytic activity under visible light. Non-metal (for example N) incorporated into TiO_2 lattice can create new valence bands through the mixing of N 2p states with O 2p states without affecting the conduction band level [4]. Many researchers performed non-metal doped-TiO_2 in a two-step fabrication approach, and the preparation process was relatively complex [1,3–6,8]. On the other hand, when TNTAs synthesized in organic electrolyte such as glycerol (14 vol% H_2O + 0.14 M NH_4F), may lead to the adsorption of this organic molecules on the TNTAs during anodic oxidation process. Annealing this as synthesized TNTAs at 450 °C for 1 h result in the incorporation of carbon element in the lattice of TNTAs (as carbon doping), since the organic molecules possibly decomposed thermally [14]. The nitrogen doped TNTAs have also been prepared by two-step in situ anodization process with ethylene glycol containing NH_4F solution as reported by Wu and coworker [15]. They reported that nitrogen incorporation in the TNTAs was supplied by the NH_4F and it was retained by annealing in dry nitrogen environment at 450 °C for 1 h. Moreover, the simple method by in-situ doping or one pot reaction resulted in better quality nanotubes than the post-treatment method as reported by Milad and co workers [16]. They studied in situ carbon doping to TNTAs with polyvinyl alcohol containing NaF as electrolyte solution and followed by annealing in air at 500 °C for 3 h. To summarize, annealing techniques were performed to produce crystalline phase and may also lead to the incorporation of dopants that already available in the electrolyte solution along the anodic oxidation process (in-situ doping). Furthermore, variation of annealing atmosphere play important role in the incorporating dopants in the lattice of TNTAs. In order to get TNTAs with specific properties (well morphology with the longer tube length at precise thickness, low band gap value with anatase crystal structure and high photoelectrochemical properties) that enhance the photocatalytic activity of the TNTAs, arrangement of water content on the specific technological variations in annealing technique is very crucial. However, to the best of our knowledge, the studies on the roles of water content and variation of annealing atmosphere in the synthesis and modification of TNTAs by in-situ doping still remain substantially missing.

In this study, we investigated the significance effects of water content in the glycerol electrolyte solution and the variations in the process annealing technique that improve the specific characteristic and photoelectrochemical properties of doped-TNTAs via in-situ anodization.

2. Materials and methods

2.1. Fabrication of TNTAs

Titanium foils (from Baoji Jinsheng Metal Material Co., 99.6% purity, 0.3 mm thickness) were used as a substance for the growth of TNTAs. Prior to anodization, the Ti sheets (3 cm × 2 cm) were first mechanically polished with a 1500 cc sandpaper in order to obtain an appropriate brittle and flat surface. Subsequently, Ti samples were degreased in a mixture of HF, HNO_3 and H_2O with a volume ratio of 1:3:6 for 2 min, rinsed in deionized water and dried under air. TNTAs were obtained by the anodic oxidation process which performed in a two electrode configuration with a Ti foil as an anode and a platinum, Pt (3 cm × 1.5 cm, thickness 1 mm) as a cathode at room temperature. The distance between the two electrodes was kept at 3.5 cm in all experiments. This distance is selected by considering the reactor size and morphology of TNTAs to be produced [17]. A direct current power supply (Escord 6030SD) was utilized to control the voltage at 30 V for 2 h. This equipment also measured the current generated as a function of time. A mixed electrolyte solution (60 ml) of glycerol (from Brataco) containing 0.5 wt.% NH_4F (Merck, 98%) with different water content (5, 10, 25 and 50 v%) were used as the electrolyte solutions and non-metal doping source in the anodization process. The selection of constant parameters such as annealing temperature [18,19], voltage [12,20–22], amount of NH_4F [11,12,22,23] and time [11,12] is based on the optimal condition as suggested by some previous studies. To homogenize the electrolyte solution in order to get TNTAs with uniform size [24] and to enhance the mobility of the ions inside the solution [19], magnetically stirring with acceleration of 150 rpm was performed along with the anodization. As-synthesized TNTAs were properly washed in distilled water and subsequently dried under air atmosphere (denoted as as-synt TNTAs). To study the effect of mode annealing, the as-synt TNTAs were then annealed in a furnace to convert the amorphous phase to the anatase phase using air (denoted as A-TNTAs) and using 20% hydrogen in an argon atmosphere (denoted as H_2-TNTAs) at 500 °C with the rate of 150 ml s^{-1}. The temperature of the furnace was raised to 500 °C with a heating rate of 9.2 °C min^{-1}, held for 3 h and cooled naturally to room temperature. TNTAs produced by anodic oxidation with 10 and 25 v% water content in the electrolyte solution were denoted as TNTAs-10 and TNTAs-25, respectively.

2.2. Characterization

The morphology of TNTAs was characterized using scanning electron microscopy (SEM) JEOL-6390A and field emission scanning electron microscopy (FESEM) FEI-Inspect F50 with accelerating voltage of 20 kV. The elemental analysis of the TNTAs was determined by the energy-dispersive X-ray spectroscopy (EDS) attached to the SEM (at 20 kV). FTIR analysis (Shimadzu IR Prastige-21) was performed to determine the functional groups present in the TNTAs. The FTIR spectra of the photocatalysts were taken over a wavenumber range of 400–4000 cm^{-1}. A UV–Vis Spectroscopy (DRS) analysis was used to calculate the energy band gap of the TNTAs samples using spectrophotometer Shimadzu 2450 type. The

spectra of the samples were recorded under ambient condition in the wavelength range of 200–900 nm. To evaluate the crystalline phase of the TNTAs, X-ray diffraction (XRD) analysis (Shimadzu 7000 X-ray diffractometer) was used. The source of the X-ray radiation was Cu Kα (λ = 0.154184 nm) over the 2θ range of 10–80°. The scan rate used for XRD analysis was set 2° min^{-1} while the accelerating voltage and the applied current were 40 kV and 30 mA, respectively. The Scherrer equation is used to estimate the crystallite sizes of the samples from FWHM (full-width at half-maximum) of XRD.

2.3. Photoelectrochemical test

Photocurrent density measurements were performed in the photoelectrocatalytic reactor consisting of a quartz cell 40 mm in height, 25 mm in diameter, and effective volume of 20 ml with a standard three-electrode configuration in with TNTAs (photoanode), a Pt wire and a saturated Ag/AgCl as working, counter and reference electrodes, respectively. The experiment was done under the conditions of UV (an 11 W UV lamp/black light, 365 nm) and visible light (a 75 W tungsten lamp, 350–800 nm) irradiation, and 0.1 M $NaNO_3$ as supporting electrolyte. All three electrodes in the reactor were connected to a computer – controlled potentiostat (Edaq/e-corder 401) to record the photocurrent generated. The potential was swept linearly at a scan rate of 100 mV s^{-1} under illumination.

3. Results and discussion

3.1. SEM/FESEM and EDS analysis

Fig. 1 shows SEM images of TNTAs produced from anodic oxidation at 30 V for 2 h in the glycerol electrolyte solution containing 0.5 wt.% NH_4F (having 5, 10, 25 and 50 v% water content) and annealed with air at 500 °C for 3 h. The currents and pH values generated during anodization process as a function of water content can be seen in Figs. 2 and 3, respectively.

TNTAs with well tubular structure was seen in the electrolyte solution with water contents of 10 and 25 v% (Fig. 1b and c). Because

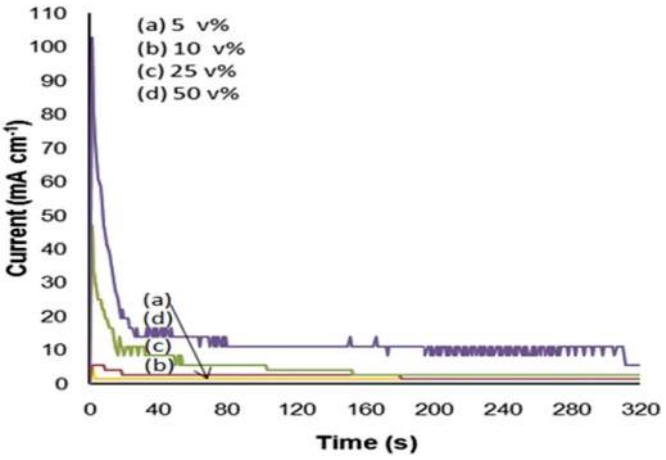

Fig. 2. The currents generated during anodization process at difference v% water content: (a) 5, (b) 10, (c) 25 and (d) 50.

of this, these two photocatalysts were selected to perform further experiments as the samples with water content of 5 and 50 v% (Fig. 1a and d), the TNTAs obtained were not well developed and relatively disordered with un-uniform diameter and thicknesses. Water content in the glycerol electrolyte solution is a crucial factor in the formation of TNTAs from titanium that can be represented in the following reaction [11,14,25]:

$$Ti + 2H_2O \rightarrow TiO_2 + 4H^+ + 4e^- \quad (1)$$

and the formation of small pits or pores due to H^+ and F^- ions (chemical dissolution of the nanotube layer if the formed metal fluorides are water-soluble) given by the reaction [11,14,25]:

$$TiO_2 + 6F^- + 4H^+ \rightarrow [TiF_6]^{2-} + 2H_2O \quad (2)$$

At lower water content (5 v%), lack of H^+ in the formation of TNTAs and high viscosity of the glycerol electrolyte solution

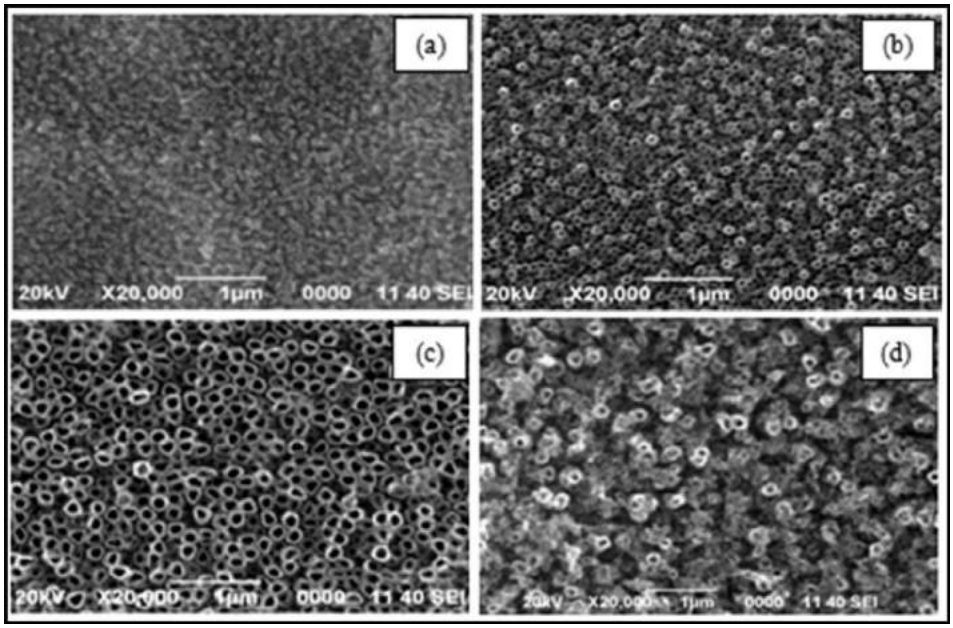

Fig. 1. Top view SEM image of TNTAs with v% water content: (a) 5, (b) 10, (c) 25 and (d) 50.

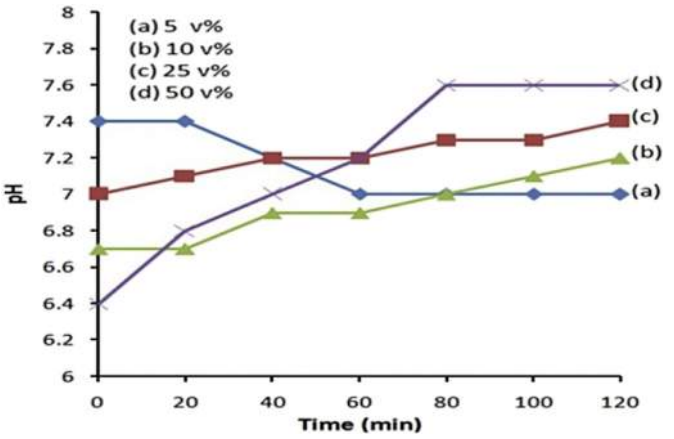

Fig. 3. The pH values during anodization process at difference v% water content: (a) 5, (b) 10, (c) 25 and (d) 50.

occurred that lead to the TNTAs structure were not observed. The presence of water in organic electrolyte was essential to form nanotubular structure according to the Eqs. (1) and (2). At higher water content (50 v%) the chemical dissolution of TNTAs occurred in a faster rate. Therefore, the TNTAs produced were disordered with un-uniform diameter and thicknesses. This phenomenon is consistent with the results reported by Yu Wang et al. [12]. They reported that at 20 and 40 wt% water content, the nanotubular structure of TNTAs were produced by anodization in glycerol electrolyte at 30 V, 2 h, pH of 6 and 40 °C. They also found that the high current generated at high water content (60, 80 and 90 wt%), resulted in the collapse of TNTAs. The higher the water content in the electrolyte solution, the more electrons could be generated (Eq. (1)), and consequently, it resulted in a higher current (Fig. 2). Moreover, as can be seen in Fig. 2, in the initial stage of anodization, the current generated decreased sharply due to the formation of dense of TiO_2.

The formation of TNTAs was also influenced by the pH and Fig. 3 shows the pH observed during anodization process at different of water content. The range pH values of TNTAs with 10 and 25 v% water content during anodization process are 6.7–7.4 (Fig. 3), where in this condition it can still provide TNTAs with morphology that its nanotube structure was self organized, well developed, ordered and uniform in diameter and thicknesses. This result is consistent with the study reported by previous researchers as at pH 6 or neutral, well-defined and highly ordered of TNTAs were formed [12,18]. The chemical dissolution rate of TNTAs is increased by lowering pH of the electrolyte solution. As a result, at lower pH (1–2), few hundred nanometers of TNTAs length was obtained [11], and flaky layer was formed [12]. Whereas, at high pH caused a low oxidation rate [12]. At pH around 5–6, longer TNTAs up to 6 μm was achieved [11]. This phenomenon is occurred since the oxidation and chemical dissolution rate reached an equilibrium and, therefore, promoted the formation of TNTAs.

The role of water content in the electrolyte solution and mode of annealing on the morphology of TNTAs can be presented in Table 1. According to Table 1, it can be seen that water content influences the dimension of TNTAs. Lower water content in the organic electrolyte decreases the availability of oxygen in the oxidation reaction of Ti to TiO_2 and results in thinner oxide barrier layers beneath the TNTAs as demonstrated by Eq. (1). In addition, it also inhibits chemical dissolution of TNTAs according to Eq. (2). Chemical dissolution occurs at the bottom of the tube, entire tube wall and the top of the tube. As a result, lower water content (Table 1) provides shorter inner diameter and tube length. Similar result is also suggested by Muhamed et al. [22]. They reported that the tube length and the diameter increased until water content reached 50 wt.% and then decreased when anodization was performed with glycerol electrolyte at 20 V, pH 6 and 1.5 h anodization time. Moreover, at low water content (TNTAs-10), the viscosity of glycerol is relatively high ($\mu = 116$ cP), therefore, the mobility/diffusion of O^{2-} and F^- ions is inhibited [22]. As a consequence, the oxidation rate (Eq. (1)) and chemical dissolution rate or pore deepening rate by F^- ion inside tube according to Eq. (2) decreases, which results in smaller diameters and shorter tube lengths.

Fig. 4 presents the role of mode annealing on the morphology of TNTAs with 25 v% water content. To obtain detailed morphology of TNTAs, the FESEM top view image at an angle of 45° and the cross section image of H_2-TNTAs with 25 v% water content (H_2-TNTAs-25) can be seen in Fig. 5. Magnetically stirring in this study is aimed to homogenize the electrolyte solution and to get TNTAs with uniform size [24]. Furthermore, this stirring can also be used to enhance mass transfer, so that, the growth rate of TNTAs could be faster [19].

Table 1 and Fig. 4 show that the mode of annealing has a less significant effect on the morphology of TNTAs as it relatively remains unchanged. However, in the form of as-synt TNTAs (amorphous phase) the inner diameter (ID) is shorter, and the tubes are covered with glycerol residue. After annealing, the inner diameter becomes larger, the tube-wall is relatively unchanged, and the glycerol residue is decomposed because of heating. In the form of amorphous phase, the TNTAs was porous and, therefore, after annealing the TNTAs become dense. As a consequence, inner diameter becomes larger. Annealing with air produced TNTAs with the spherical shape, whereas annealing with H_2 produced TNTAs with the oval shape. Fig. 5 indicates that the self-organized and ordered TNTAs are perpendicular to the Ti substrate. The EDS analysis of the as-synt TNTAs, A-TNTAs and H_2-TNTAs with 10 and 25 v% water content in the electrolyte solution indicated that the main elements present in the TNTAs were Ti and O, however, C, N and F were also detected since they were adsorbed during the anodization process and stayed on the surface of TNTAs. Carbon could be supplied by glycerol [14], whereas N could be supplied by NH_4F [15], and F could be supplied by NH_4F. Annealing at 500 °C for 3 h leads to internal diffusion of carbon and nitrogen into TNTAs lattice. These non-metals can substitute or only adsorbed and bonded to oxygen atoms in TNTAs. To verify the incorporation of these elements in the matrix of TNTAs, FTIR analysis was performed.

Table 1
The average of inner diameter, wall thickness and length of TNTAs for different water content and mode of annealing.

Photocatalyst	TNTAs-10 ($\mu = 116$ cP)			TNTAs-25 ($\mu = 24$ cP)		
	ID[a] (nm)	t[b] (nm)	L[c] (nm)	ID[a] (nm)	t[b] (nm)	L[c] (nm)
As-synt TNTAs	33	33		58	31	
A-TNTAs	52	32	1407	78	42	1570
H_2-TNTAs	49	28		80	33	

[a] Average inner diameter.
[b] Average wall thickness.
[c] Average length of TNTAs.

3.2. FTIR analysis

The functional groups present in as-synt TNTAs, A-TNTAs and H_2-TNTAs photocatalysts (10 v% water content) which are identified by characteristic peaks in transmission spectra in the 4000–400 cm^{-1} are depicted in Fig. 6. Similar results were also obtained for other photocatalysts with 25 v% water content (figure

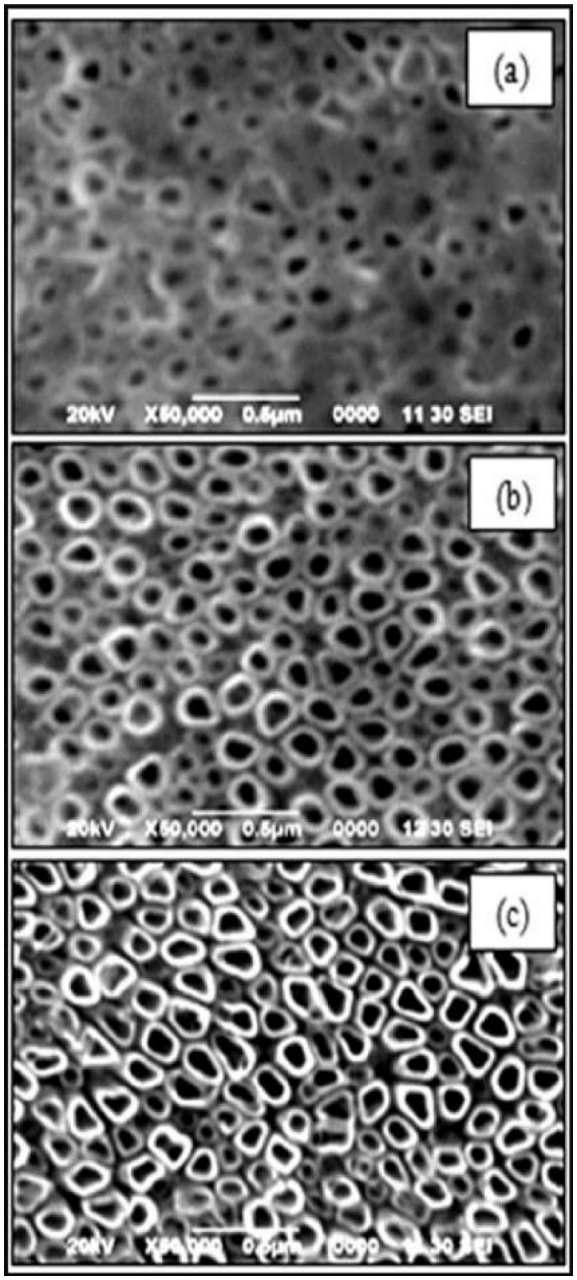

Fig. 4. SEM image of (a) as-synt TNTAs (b) A-TNTAs and (c) H_2-TNTAs with 25 v% water content in the electrolyte solution.

not presented). The transmission peaks at around 3700 cm^{-1} and 1550 cm^{-1} correspond to the O–H stretching of the hydroxyl group to Ti atoms and O–H bending vibration (surface adsorbed water molecules), respectively [5,6,26]. The IR bands were observed to be less than 1000 cm^{-1} (840 and 420 cm^{-1}) correspond to the Ti–O and Ti–O–Ti stretching vibrations of crystalline TiO_2 [5,6,27]; therefore, these peaks were not observed in the as-synt TNTA as it has an amorphous phase. Annealing helps in the incorporating of dopant in the lattice of TNTAs. As a result, the peaks at around 1050 cm^{-1} and a very weak peak at around 1200 cm^{-1} in A-TNTAs and H_2-TNTAs are assigned for N–Ti–O bond (substitutional N doping in the lattice of TNTAs) [6] and Ti–O–C bond (interstitial C doping in the TNTAs) respectively [28,29]. Thus, these two peaks were not found in the amorphous phase of TNTAs (Fig. 6a). The weak absorption peaks at 2344–2349 cm^{-1} (Fig. 6a–c) are the character of N–H stretching vibration [5]. In this study, the presence of F is not clearly identified by the FTIR analysis as also reported by Lee et al. [30] since the peak at around 889 cm^{-1} that attributed to Ti–F vibration (substitutional F doping in the lattice of TNTAs) was not observed [31].

In this work, when the as-synt TNTAs were annealed under H_2/Ar, the color changed from gray to dark blue. This change is associated with the reduction of Ti^{4+} to Ti^{3+} [18,32]. As a result, O_2 liberated from TiO_2 and caused an O_2 vacancy which can be substituted by Nitrogen to form an N–Ti–O bond. The N–Ti–O bond also was observed when as-synt TNTAs was annealed by air. This may be attributed to the substitutional doping of N, and it was retained when annealing with nitrogen environment in air. The formation of Ti–O–C or N–Ti–O bond characterized by FTIR indicated that C and N already doped through either adsorbed and bonded to oxygen atoms or through replacement of the oxygen atoms in the matrix of TNTAs. A schematic sketch of the model of carbon or nitrogen doping can be depicted in Fig. 7 [33].

As C and N were doped in the TNTAs, UV–Vis DRS analysis was performed to calculate the band gap energy.

3.3. UV–Vis DRS spectra analysis

The band gap energy (Eg) of photocatalyst is calculated by applying Kubelka–Munk function F(R) and Tauc plot. That formula is:

$$[F(R)\cdot h\nu]^{1/2} = K(h\nu - Eg) \quad (3)$$

where $F(R) = (1 - R)^2/2R$, R = reflectance, $h\nu$ = photon energy and K = constant characteristic of TiO_2.

For the semiconductor TiO_2, a plot of $[F(R)\cdot h\nu]^{1/2}$ vs. $h\nu$ should show a linear region just above the optical absorption edge [5,34]. The extrapolation of the linear portion of a Tauc plot to the $h\nu$ axis results in the band gap energy of photocatalyst as can be depicted in Fig. 8.

As shown in Fig. 8a–d, all of the photocatalysts undergo band gap reduction and for TiO_2–P25 film, the band gap is 3.3 eV that is similar to that of TiO_2 anatase. Compared to the A-TNTAs (band gap 2.8 and 3 eV), the H_2-TNTAs (band gap 2.2 and 2.7 eV) show better absorption in the visible region. This result is accordance with that of Mohapatra et al. [19,23]. They reported that annealing under H_2 on TNTAs at 625 °C for 60 min resulted by anodization process in ethylene glycol electrolyte solution gave maximum absorbance in the visible region as the band gap can be reduced to around 2.0 eV. It means that, annealing with the H_2/Ar can suppress the oxidation reaction of elements C, N and F that present in the surface of amorphous TNTAs and those elements were incorporated in the lattice of TNTAs during annealing process. In other words, the incorporated of those elements were possibly retained by H_2/Ar. Furthermore, during inert-gas annealing (for example Ar) or annealing with reducing conditions (for example H_2), unsaturated titanium (Ti^{3+}) states or O_2 vacancies could be generated on the surface of TNTAs [18,32] that allowed substitutional doping of N. Annealing N-doped TNTAs at high temperatures in an oxygen-rich environment usually removes the nitrogen by oxidation [15], therefore, the A-TNTAs have higher band gap than H_2-TNTAs. Reducing the band gap may be attributed to the substitutional N doping and interstitial C doping in A/H_2-TNTAs matrix to form N–Ti–O and Ti–O–C bonds, which are responsible for the red shift in the absorption band [3–6,19,23]. However, substitutional doping is more influential than interstitial doping [19]. From this analysis, the optimum condition for photocatalysis in this study is H_2-TNTAs-10 with a band gap energy of 2.2 eV, since it can more absorb the visible light.

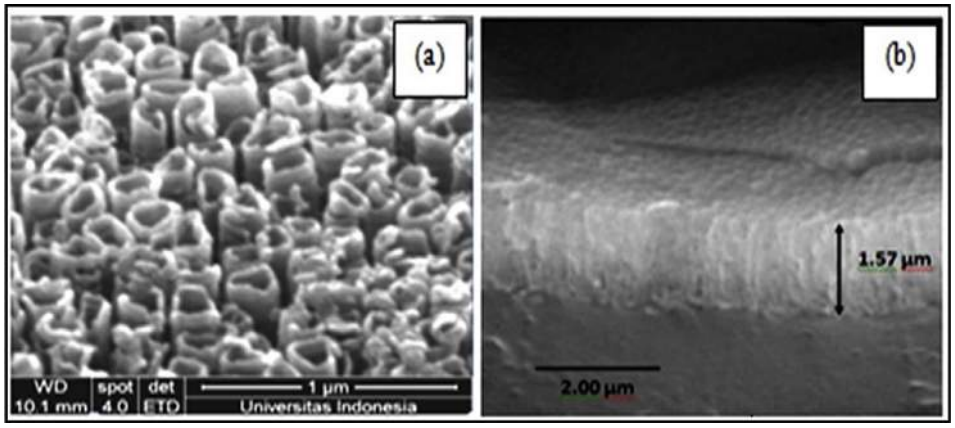

Fig. 5. FESEM (a) top view image with angle 45° and (b) cross section image of H_2-TNTAs-25.

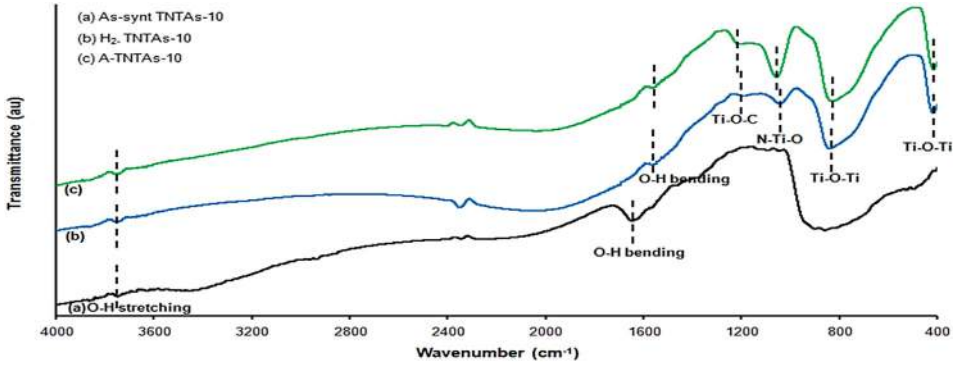

Fig. 6. The FTIR spectra of (a) as-synt TNTAs, (b) H_2-TNTAs, (c) A-TNTAs with 10 v% water content in the electrolyte solution.

3.4. XRD patterns analysis

The XRD patterns of TiO_2—P25, as-synt TNTAs, H_2-TNTAs-25, H_2-TNTAs-10 and A-TNTAs-25 are summarized in Fig. 9. Fig. 9b illustrates XRD pattern of the as-synt TNTAs (before annealing) and therefore no anatase or rutile crystalline phases were observed as it has amorphous phase. Annealing as-synt TNTAs at 500 °C for 3 h produced anatase (A) phase. Higher temperatures can cause the anatase to transform into rutile (R) [18]. The H_2-TNTAs-25, H_2-TNTAs-10 and A-TNTAs-25 (Fig. 9c, d and e) gave peaks in the 2θ at 25.3°, 37.9°, 48,04°, 54.04°, 55.09° which are the diffraction of the field (101), (004), (200), (105), (221) of the anatase TNTAs (JCPDS card No.21-1272), while the crystallite size calculated by the Scherrer equation [7] are 22, 27 and 33 nm, respectively. With annealing, the degree of crystalline and crystallite size increase which is assigned with the increasing intensity and narrowing the FWHM. Annealing with air (A-TNTAs-25) resulted in sharper, and

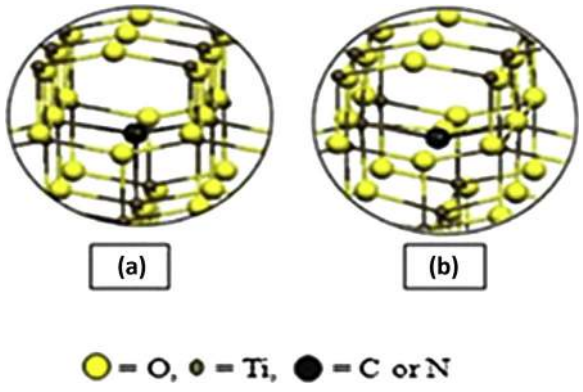

Fig. 7. A schematic sketch of the model for (a) substitutional and (b) interstitial C or N doping in TNTAs (Reprinted with permission from ref. [33] ©2005 American Chemical Society).

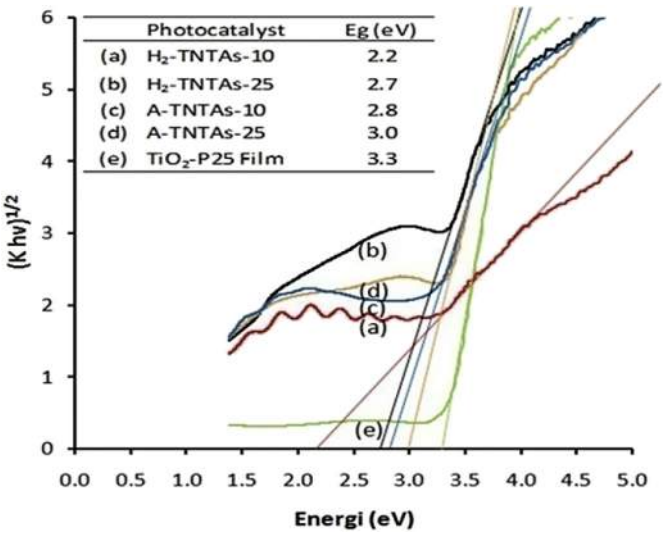

Fig. 8. Tauc plot of transformed Kubelka–Munk function vs. hv for various photocatalysts.

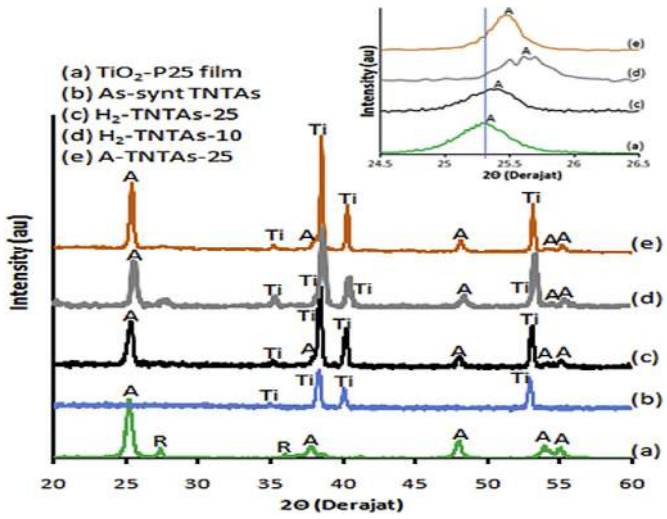

Fig. 9. The XRD patterns of (a) TiO_2—P25 film, b) As-synt TNTAs, (c) H_2-TNTAs-25, (d) H_2-TNTAs-10 and (e) A-TNTAs-25.

higher the peak of anatase phase (in the 2θ at 25.3°) compare to other samples; therefore, it has bigger crystallite size (33 nm). Since the crystallite size of H_2-TNTAs-25 is smaller than the two others, its photocatalyst activity and its stability in the anatase phase would be better [15]. In this study, the change in d-spacing also was observed since dopants (C and N) were incorporated in the TNTAs lattice (inset Fig. 9). The diffraction peaks for the C/N or C/N containing phases were not detected, indicating that those atoms were highly dispersed on TiO_2 or possibly its content on the TiO_2 surface is not enough to form crystalline [6,26]. It may imply that carbon and nitrogen are incorporated into TNTAs. For the TiO_2—P25, 79 wt.% of anatase was obtained with crystallite sizes of anatase and rutile are 20 and 23 nm, respectively.

3.5. Photoelectrochemical test

The photocurrent density vs. applied potential curves of the TNTAs photoanode in 0.1 M $NaNO_3$ electrolyte in the UV light illumination, are shown in Fig. 10. The observed dark current density was found to be negligible as close to zero. The currents resulted from various photocatalyst with an area of 2 cm^2 and applied potential at 1 V are depicted in Table 2.

All photocatalysts (Fig. 10 and Table 2) show that A-TNTAs and

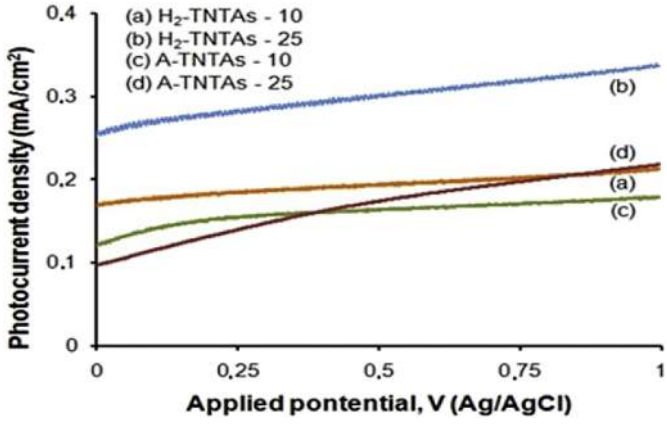

Fig. 10. Photocurrent density vs. applied potential of (a) H_2-TNTAs-10, b) H_2-TNTAs-25 (c) A-TNTAs-10 and (d) A-TNTAs-25 in UV light illumination.

H_2-TNTAs are responsive to the UV and visible illumination. This result is in accordance with that of UV—Vis DRS as all samples underwent a lowering of the band gap energy. According to Table 2, the currents produced by H_2-TNTAs-25 and H_2-TNTAs-10 under visible light illumination (0.086 and 0.074 mA/cm^2) are higher than that of A-TNTAs-25 and A-TNTAs-10 (0.062 and 0.058 mA/cm^2). Theoretically, the H_2-TNTAs-10, which has the lowest band gap (2.2 eV), provided the highest photocurrent to visible light. However, the photocurrent generated is lower than that of H_2-TNTAs-25 (2.7 eV) (Table 2). This is because, the photocurrent is influenced by electrons—hole's recombination if the band gap is too small [35]. In addition, it is also influenced by length and wall thickness of the nanotube [36,37]. In this study, the tube length of TNTAs-25 (1570 nm) is longer than that of TNTAs-10 (1407 nm), therefore, more photons can be absorbed by TNTAs-25. As a result, the photocurrent of TNTAs-25 increases. Moreover, the wall thickness of H_2-TNTAs-25 (33 nm) showed a higher photocatalyst activity than A-TNTAs-25 (42 nm). It means that, the recombination of electrons—holes in H_2-TNTAs-25 can be suppressed since the width of space charge layer of H_2-TNTAs-25 is near to its wall thickness. A-TNTAs-25 with thicker wall thickness provides lower photocurrent density as its wall thickness larger than the width of the space charge layer. As a result, transfer electrons to the counter electrode (Pt) and holes to the surface of TNTAs are restricted due to the longer path to go through. Therefore, recombination occurs readily. For the TNTAs, electrons and holes (e^- and h^+) are produced at entire inner tube wall and two side of outer tube wall, which consists of space charge layers. With external bias, electrons move to the bulk of TNTAs, and then transfer to the counter electrode (Pt), whereas holes move to the surface of TNTAs (electrolyte solution). Higher photocurrent or higher photoelectrocatalytic activity means that the photo-induced electrons transfer from working electrodes (TNTAs) to the counter electrode (Pt) is higher than the recombination of photogenerated electrons and holes [3,37]. In the previous study, the addition of $NaBF_4$ as electrolytes during TNTAs formation process, resulting to an insitu doping, and eventually lead to produce a photocatalyst that was able to suppress recombination [38]. The optimum photocurrent response was observed for H_2-TNTAs-25, which indicated that the band gap optimum for photocatalysis (2.7 eV) was achieved. This phenomenon is occurred since H_2-TNTAs-25 has longer the tube, lower recombination and smaller crystallite size than other photocatalysts.

4. Conclusion

The morphology and dimensions of TiO_2 nanotube arrays (TNTAs) is optimized by varying water content in the electrolyte solution. Specific properties of the TNTAs such as well developed tubes, vertically oriented, highly ordered, long with certain diameter and wall thickness is optimized by varying water content. At lower water content, the structure of TNTAs were not observed, indicated that the morphology of TNTAs were not well developed. In contrast, higher water content resulted in TNTAs with morphology disorder as well as un-uniform in diameter and

Table 2
The photocurrent generated by H_2-TNTAs and A-TNTAs with deferent water content at 1 V vs. Ag/AgCl).

Photocatalysts	Current, mA/cm^2	
	Vis	UV
H_2-TNTAs-10	0.074	0.213
H_2-TNTAs-25	0.086	0.337
A-TNTAs-10	0.058	0.179
A-TNTAs-25	0.062	0.218

thicknesses. The technological variations in annealing technique significantly affect the improvement of doped-TNTAs properties. Annealing of as-synt TNTAs under air or H_2/Ar is not only converting amorphous to anatase phase, but also helping in incorporating carbon/nitrogen to the lattice of TNTAs. Therefore, carbon/nitrogen-doped TNTAs were obtained by in-situ anodic oxidation with glycerol containing NH_4F solution as the electrolyte solution. Meanwhile, the possibility of dopant C or N incorporated in TNTAs to form of Ti–O–C or N–Ti–O bonds can be confirmed by FTIR analysis. It was also demonstrated that H_2-TNTAs have lower band gaps compared to A-TNTAs since annealing with air could oxidize the dopant that present in the TNTAs. Additionally, annealing with H_2/Ar could cause the reduction of Ti^{4+} to Ti^{3+}, allowing nitrogen to substitute oxygen in the matrix of TiO_2. According to the current density measurement, H_2-TNTAs-25 exhibited the optimum photocatalyst performance compared to the H_2-TNTAs-10. This is because, certained morphology of TNTAs with the specific annealing could enhance the photoelectrochemical response of TNTAs.

Acknowledgment

The authors would like to thank the LP3M Indonesia Institute of Technology and Directorate General of Higher Education (DGHE), Indonesian Ministry of National Education for the financial support of this research (Hibah Bersaing grant no. 025/K3/KM/SPK/2013).

References

[1] Slamet, D. Tristantini, Valentina, M. Ibadurohman, Int. J. Energy Res. 37 (2013) 1372.
[2] R. Khan, S.W. Kim, T.J. Kim, C.M. Nam, Mater. Chem. Phys. 112 (2008) 167.
[3] G. Yan, M. Zhang, J. Hou, J. Yang, Mater. Chem. Phys. 129 (2011) 553.
[4] P. Wang, T. Zhou, R. Wang, T.T. Lim, Water Res. 45 (2011) 5015.
[5] L. Zhou, J. Deng, Y. Zhao, W. Liu, L. An, F. Chen, Mater. Chem. Phys. 117 (2009) 522.
[6] Y.L. Pang, A.Z. Abdullah, Chem. Eng. J. 214 (2013) 129.
[7] V. Stengl, S. Bakardjieva, N. Murafa, Mater. Chem. Phys. 114 (2009) 217.
[8] Y. Wu, M. Xing, J. Zhang, F. Chen, Appl. Catal. B Environ. 97 (2010) 182.
[9] Y. Lee, M. Kang, Mater. Chem. Phys. 122 (2010) 284.
[10] C.J. Liu, T.Y. Yang, C.H. Wang, C.C. Chien, S.T. Chen, C.L. Wang, W.H. Leng, Y. Hwu, H.M. Lin, Y.C. Lee, C.L. Cheng, J.H. Je, G. Margaritondo, Mater. Chem. Phys. 117 (2009) 74.
[11] A.E.R. Mohamed, S. Rohani, Energy Environ. Sci. 4 (2011) 1065.
[12] Y.W. Wen, B.R. Chen, Int. J. Photoenergy (2013), http://dx.doi.org/10.1155/2013/348171. Article ID 34817.
[13] X. Liu, Z. Liu, J. Zheng, X. Yan, D. Li, S. Chen, W. Chu, J. Alloys Compd. 509 (2011) 9970.
[14] F.M.B. Hassan, H. Nanjo, S. Venkatachalam, M. Kanakubo, T. Ebina, J. Power Sources 195 (2010) 5889.
[15] H. Wu, Z. Zhang, Int. J. Hydrog. Energy 36 (2011) 1348.
[16] A.M. Milad, M.B. Kassim, W.R. Daud, WASET 74 (2011) 171.
[17] S. Yoriya, Int. J. Electrochem. Sci. 7 (2012) 9454.
[18] P. Roy, S. Berger, P. Schmuki, Angew. Chem. Int. Ed. 50 (2011) 2904.
[19] S.K. Mohapatra, M. Misra, V.K. Mahajam, K.S. Raja, J. Catal. 246 (2007) 362.
[20] C.W. Lai, S. Sreekantan, Int. J. Photoenergy (2011), http://dx.doi.org/10.1155/2011/142463. Article ID 142463.
[21] J.M. Macak, H. Tsuchiya, A. Ghicov, K. Yasuda, R. Hahn, S. Bauer, P. Schmuki, Solid State Mater. Sci. 11 (2007) 3.
[22] A.E.R. Mohamed, S. Rohani, AIDIC Conf. Ser. 9 (2009), http://dx.doi.org/10.3303/ACOS0909015.
[23] S.K. Mohapatra, M. Misra, V.K. Mahajan, K.S. Raja, J. Phys. Chem. C 111 (2007) 8677.
[24] P.M. Perillo, F. Rodriguez, Nanosci. Methods 1 (2012) 194.
[25] J. Bai, B. Zhou, L. Li, Y. Liu, J. Mater. Sci. 43 (2008) 1880.
[26] L. Liang, Y. Yulin, L. Xinrong, F. Ruiqing, S. Yan, L. Shuo, Z. Lingyun, F. Xiao, T. Pengxiao, X. Rui, Z. Wenzhi, W. Yazhen, M. Liqun, Appl. Surf. Sci. 265 (2013) 36.
[27] F. Chekin, S. Bagheri, S.S.A. Hamid, Sens. Actuat. B Chem. 177 (2013) 898.
[28] R. Parra, M.S. Goes, M.S. Castro, E. Longo, P.R. Bueno, J.A. Varela, Chem. Mater. 20 (2008) 143.
[29] S. Sener, M. Erdemoglu, M. Asilturk, H. Sayilkan, Turk. J. Chem. 29 (2005) 487.
[30] Y.S. Lee, S.J. Kim, P. Venkateswaran, J.S. Jang, H. Kim, J.G. Kim, Carbon Lett. 9 (2008) 131.
[31] D. Huang, S. Liao, S. Quan, L. Liu, Z. He, J. Wan, et al., J. Mater. Sci. 42 (2007) 8193.
[32] M.S. Hamdy, R. Amrollahi, G. Mul, ACS Catal. 2 (2012) 2641.
[33] C.D. Valentin, G. Pacchioni, A. Selloni, S. Livraghi, E. Gimello, J. Phys. Chem. B 109 (2005) 11414.
[34] L.S. Yoong, F.K. Chong, B.K. Dutta, Energy XXX (2009) 1.
[35] J. Xiang, T. Nathan-Wallesser, IJMSCI 3 (2013) 104.
[36] J.H. Park, S. Kim, A.J. Bard, Nano Lett. 6 (2006) 24.
[37] C.W. Lai, S. Sreekantan, Int. J. Photoenergy (2012), http://dx.doi.org/10.1155/2012/356943. Article ID 356943.
[38] Ratnawati, J. Gunlazuardi, E.L. Dewi, Slamet, Int. J. Hydrog. Energy 39 (2014) 16927.